Available online at www.sciencedirect.com
SCIENCE DIRECT®
International Journal of Solids and Structures 42 (2005) 4890–4908
INTERNATIONAL JOURNAL OF SOLIDS and STRUCTURES
www.elsevier.com/locate/ijsolstr

Intensity of singular stress at the fiber end in a hexagonal array of fibers

Nao-Aki Noda *, Yasushi Takase

Kyushu Institute of Technology, Department of Mechanical Engineering, 1-1 Sensui-cho, Tobata-ku, Kitakyushu 804-8550, Japan

Available online 21 March 2005

Abstract

To evaluate the mechanical strength of fiber-reinforced composites it is necessary to consider singular stresses at the end of fibers because they cause crack initiation, propagation, and final failure. The singular stress field is controlled by generalized stress intensity factor (GSIF) defined at the fiber end. In this study, periodic and zigzag arrays of cylindrical inclusions under longitudinal tension are considered in comparison with the results for a single fiber. The unit cell region is approximated as an axi-symmetric cell; then, the body force method is applied, which requires the stress and displacement fields due to ring forces in infinite bodies having the same elastic constants as those of the matrix and inclusions. The given problem is solved on the superposition of two auxiliary problems under different boundary conditions. To obtain the GSIF accurately, the unknown body force densities are expressed as piecewise smooth functions using fundamental densities and power series. Here, the fundamental densities are chosen to represent the symmetric stress singularity, and the skew-symmetric stress singularity. The GSIFs are systematically calculated with varying the elastic modulus ratio and spacing of fibers. The effects of volume fraction and spacing of fibers are discussed in fiber-reinforced plastics.

Keywords: Elasticity; Composite material; Fracture mechanics; Body force method; Generalized stress intensity factor; Hexagonal array; Zigzag array; Cylindrical inclusion; Reinforced plastics

1. Introduction

To evaluate the mechanical strength of fiber-reinforced composites it is necessary to consider singular stresses at the end of fibers because they cause crack initiation, propagation, and final failure (Nisitani et al., 1993). Consider a cylindrical inclusion with a local polar coordinate as shown in Fig. 1 as a model

* Corresponding author. Tel./fax: +81 93 884 3124.
E-mail address: noda@mech.kyutech.ac.jp (N.-A. Noda).

0020-7683/$ - see front matter © 2005 Elsevier Ltd. All rights reserved.
doi:10.1016/j.ijsolstr.2005.01.021

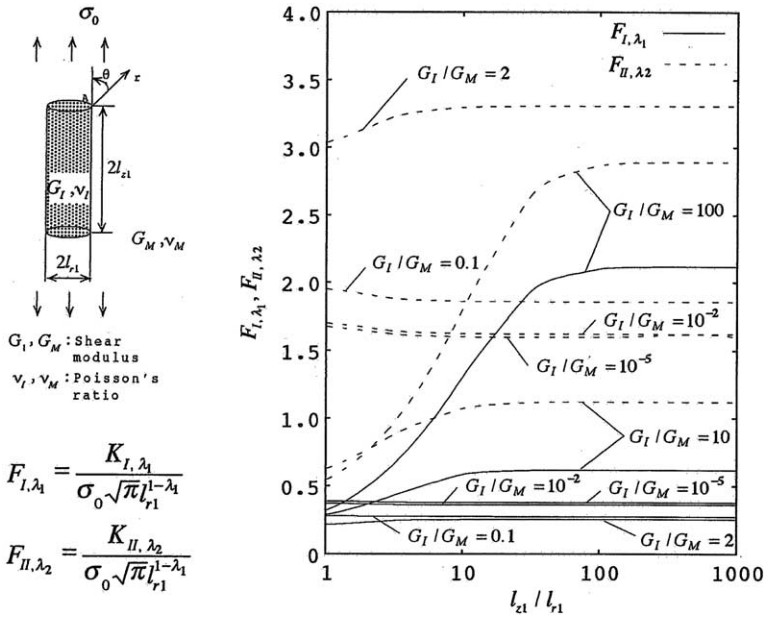

Fig. 1. Generalized stress intensity factors for a single fiber when $\nu_1 = \nu_M = 0.3 (F_{I,\lambda_1} = K_{I,\lambda_1}/(\sigma_0\sqrt{\pi} l_1^{1-\lambda_1}), F_{II,\lambda_2} = K_{II,\lambda_2}/(\sigma_0\sqrt{\pi} l_1^{1-\lambda_2}))$.

of fiber. Then, the singular stress around the corner of an inclusion can be expressed by the following equations (Chen and Nisitani, 1993; Noda et al., 2003). Here, the generalized stress intensity factors $K_{I,\lambda 1}$, $K_{II,\lambda 2}$ can be regarded as an extension of the ordinary stress intensity factors, which are usually defined for cracks, to inclusion corners.

$$\sigma_{\theta,i} = \frac{K_{I,\lambda_1}}{r^{1-\lambda_1}} f^{I}_{\theta,i}(\theta) + \frac{K_{II,\lambda_2}}{r^{1-\lambda_2}} f^{II}_{\theta,i}(\theta) \quad (i = 1, 2) \tag{1}$$

For matrix ($i = 1$): $-3\pi/4 \leqslant \theta \leqslant 3\pi/4$

$$\begin{aligned} f^{I}_{\theta,1}(\theta) = & \frac{\lambda_1}{\sqrt{2\pi}(\alpha-\beta)} ([-\lambda_1(\alpha-\beta)\cos(\lambda_1\pi/2) + (1-\beta)\sin(\lambda_1\pi)] \\ & \times \cos\{(\lambda_1+1)\theta\} + [(\lambda_1+1)(\alpha-\beta)\sin(\lambda_1\pi/2)] \times \cos\{(\lambda_1-1)\theta\}) \\ f^{II}_{\theta,1}(\theta) = & \frac{\lambda_2}{\sqrt{2\pi}(\alpha-\beta)} ([-\lambda_2(\alpha-\beta)\cos(\lambda_2\pi/2) - (1-\beta)\sin(\lambda_2\pi)] \\ & \times \sin\{(\lambda_2+1)\theta\} + [(\lambda_2+1)(\alpha-\beta)\sin(\lambda_2\pi/2)] \times \sin\{(\lambda_2-1)\theta\}) \end{aligned} \tag{2a}$$

For inclusion ($i = 2$): $\theta \leqslant -3\pi/4$, $\theta \geqslant 3\pi/4$

$$\begin{aligned} f^{I}_{\theta,2}(\theta) = & \frac{-C_1\lambda_1}{\sqrt{2\pi}(\alpha-\beta)} ([-\lambda_1(\alpha-\beta)\cos(\lambda_1\pi/2) + (1-\beta)\sin(\lambda_1\pi)] \\ & \times \cos\{(\lambda_1+1)(\pi-\theta)\} + [(\lambda_1+1)(\alpha-\beta)\sin(\lambda_1\pi/2)] \times \cos\{(\lambda_1-1)(\pi-\theta)\}) \\ f^{II}_{\theta,2}(\theta) = & \frac{C_2\lambda_2}{\sqrt{2\pi}(\alpha-\beta)} ([\lambda_2(\alpha-\beta)\cos(\lambda_2\pi/2) - (1-\beta)\sin(\lambda_2\pi)] \\ & \times \sin\{(\lambda_2+1)(\pi-\theta)\} + [(\lambda_2+1)(\alpha-\beta)\sin(\lambda_2\pi/2)] \times \sin\{(\lambda_2-1)(\pi-\theta)\}) \end{aligned} \tag{2b}$$

Here,

$$C_1 = \frac{(1-\beta)\sin\{\lambda_1\gamma\} + (1-\alpha)\sin\{\lambda_1(\pi-\gamma)\} + \lambda_1(\alpha-\beta)\sin\gamma}{(1+\beta)\sin\{\lambda_1(2\pi-\gamma)\} + (1+\alpha)\sin\{\lambda_1(\gamma-\pi)\} + \lambda_1(\alpha-\beta)\sin\gamma}$$
$$C_2 = \frac{(1-\beta)\sin\{\lambda_2\gamma\} + (1-\alpha)\sin\{\lambda_2(\pi-\gamma)\} - \lambda_2(\alpha-\beta)\sin\gamma}{(1+\beta)\sin\{\lambda_2(2\pi-\gamma)\} + (1+\alpha)\sin\{\lambda_2(\gamma-\pi)\} - \lambda_2(\alpha-\beta)\sin\gamma} \tag{2c}$$

$$\alpha = \frac{G_{\mathrm{I}}(\kappa_{\mathrm{M}}+1) - G_{\mathrm{M}}(\kappa_{\mathrm{I}}+1)}{G_{\mathrm{I}}(\kappa_{\mathrm{M}}+1) + G_{\mathrm{M}}(\kappa_{\mathrm{I}}+1)}, \quad \beta = \frac{G_{\mathrm{I}}(\kappa_{\mathrm{M}}-1) - G_{\mathrm{M}}(\kappa_{\mathrm{I}}-1)}{G_{\mathrm{I}}(\kappa_{\mathrm{M}}+1) + G_{\mathrm{M}}(\kappa_{\mathrm{I}}+1)} \tag{2d}$$

where

$$\kappa_i = \frac{(3-\nu_i)}{(1+\nu_i)} \quad \text{(for plane stress)},$$
$$\kappa_i = 3 - 4\nu_i \quad \text{(for plane strain)}, \quad (i = \mathrm{M}, \mathrm{I}) \tag{2e}$$

In these equations, α, β are Dundurs parameters (Dundurs, 1967), and (G_{M}, ν_{M}) and (G_{I}, ν_{I}) are shear modulus and Poisson's ratio of the matrix and inclusion, respectively. Quite a few studies have been made for singular stresses at the fiber ends (Christman et al., 1989; Tvergaard, 1990). However, little attention has been paid to the generalized stress intensity factors as shown in Eq. (1) because usually it is very difficult to obtain them by using ordinary numerical procedure using such as finite element techniques. Fig. 1 shows generalized stress intensity factors at a fiber end when a single fiber is in matrix (Noda et al., 2003). In Fig. 1, λ_1, λ_2 are the root of the following eigenequation (Bogy and Wang, 1971; Chen and Nisitani, 1993).

For mode I

$$\begin{aligned} D_1(\alpha,\beta,\gamma,\lambda) = {} & (\alpha-\beta)^2\lambda^2(1-\cos 2\gamma) + 2\lambda(\alpha-\beta)\sin\gamma\{\sin\lambda\gamma + \sin(2\pi-\gamma)\} \\ & + 2\lambda(\alpha-\beta)\beta\sin\gamma\{\sin\lambda(2\pi-\gamma) - \sin\lambda\gamma\} + (1-\alpha^2) - (1-\beta^2)\cos 2\lambda\pi \\ & + (\alpha^2-\beta^2)\cos\{2\lambda(\gamma-\pi)\} = 0 \end{aligned} \tag{3}$$

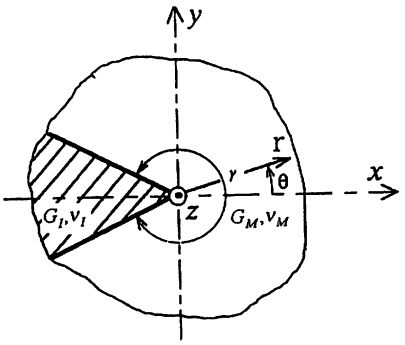

Fig. 2. Singular stress fields near the tip of a V-notch.

For mode II

$$D_2(\alpha,\beta,\gamma,\lambda) = (\alpha-\beta)^2\lambda^2(1-\cos 2\gamma) + 2\lambda(\alpha-\beta)\sin\gamma\{\sin(2\pi-\gamma)+\sin\lambda\gamma\} - 2\lambda(\alpha-\beta)\beta\sin\gamma\{\sin\lambda(2\pi-\gamma)-\sin\lambda\gamma\} + (1-\alpha^2)-(1-\beta^2)\cos 2\lambda\pi + (\alpha^2-\beta^2)\cos\{2\lambda(\gamma-\pi)\} = 0 \quad (4)$$

Here, λ_1 is a real root of Eq. (1), and λ_2 is a real root of Eq. (2). In the vicinity of inclusion corners, plane strain conditions can be assumed. Then, in this paper, we can put $\gamma = 3\pi/2$ (see Fig. 2 and the corner of cylindrical inclusion in Fig. 1).

Since actual composites usually have many fibers, in this paper, periodic and zigzag arrays of cylindrical inclusions under longitudinal tension are considered as models of many fibers (see Fig. 3). Then, the unit cell region is approximated as an axi-symmetric cell as shown in Fig. 3(c), where the body force method of analysis (Nisitani, 1967) will be applied.

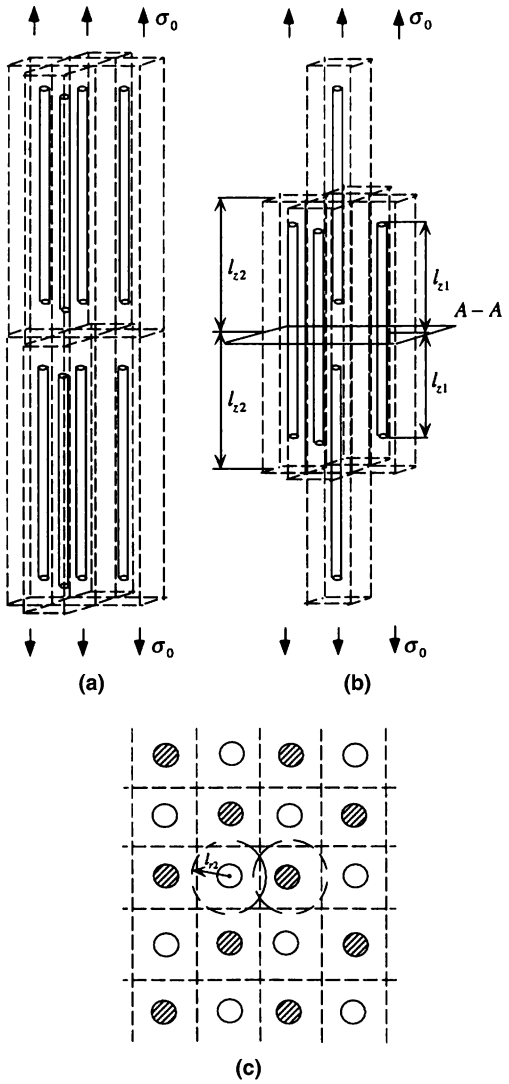

Fig. 3. Unit cell model for 3D arrays of inclusions: (a) periodic array, (b) zigzag array and (c) axi-symmetric approximation.

Here, the body force method is based on superposition of the stress field due to point force. Then, the problem is formulated as a system of singular integral equations, where the unknown functions are the densities of body forces distributed in infinite bodies having the same elastic constants as those of the matrix and inclusions. The unknown functions are expressed as piecewise smooth functions using two types of fundamental densities and power series, where the fundamental densities are chosen to express singular stresses field exactly. Then, generalized stress intensity factors K_{I,λ_1} and $K_{\mathrm{II},\lambda_2}$ at the fiber end are systematically calculated with varying the elastic ratio $G_{\mathrm{I}}/G_{\mathrm{M}}$, and aspect ratio of the unit cell l_{z2}/l_{r2} and volume fraction of fibers $V_f = \left(l_{r1}^2 l_{z1}\right)/\left(l_{r2}^2 l_{z2}\right)$ (see Fig. 4).

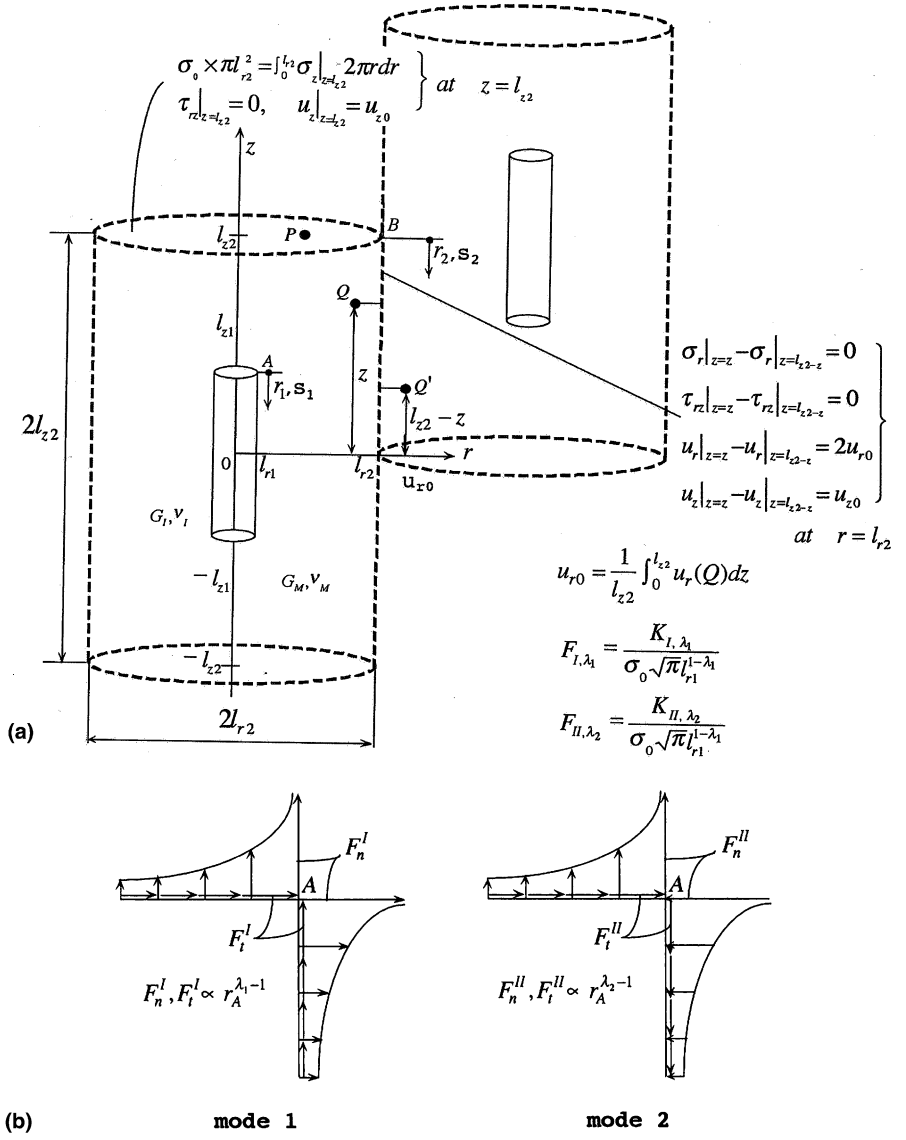

Fig. 4. (a) A cylindrical inclusion in a unit cell (u_{r0}: average displacement at $r = l_{r2}$, u_{z0}: constant displacement at $z = l_{z2}$). (b) Body force distributed around the corner A (similar body force also distributed around the corner B).

2. Singular integral equations of the body force method

In the previous study, the generalized stress intensity factors at a fiber end of a single fiber was studied (Noda et al., 2003). In this paper, therefore, the method of analysis for arrays of fibers will be discussed. Here, a zigzag array of cylindrical inclusions is taken as an example; then, the method of analysis will be explained. The unit cell model in Fig. 3(b) can be analyzed in the following procedure. Here, l_{r1} and l_{z1} are dimensions of inclusion in the r- and z-directions, respectively (see Fig. 3). Also, l_{r2} and l_{z2} are dimensions of unit cell in the r- and z-directions, u_{r0} is an average displacement at $r = l_{r2}$ (see the definition in Fig. 4), u_{z0} is a constant displacement at $z = l_{z2}$. Denote the shear modulus and Poisson's ratios of the matrix by (G_{M}, ν_{M}) and the ones of the inclusions by (G_{I}, ν_{I}). Assume two infinite bodies 'M' and 'I' have the same elastic constants of the ones of matrix and inclusions, respectively (see Fig. 4). On the idea of the body force method, the problem is formulated as a system of singular integral equations as shown in Eqs. (5) and (6). Here, there are four types of unknown functions, that is,

(A) Body forces densities F_{nM1}, F_{tM1} distributed in the normal and tangential directions along the fictitious boundary for inclusion in body 'M',
(B) Body forces densities F_{nI1}, F_{tI1} distributed in the normal and tangential directions along the fictitious boundary for inclusion in body 'I', and
(C) Body forces densities F_{nM2}, F_{tM2} distributed in the normal and tangential directions along the fictitious boundary for unit cell in body 'M'.
(D) Body forces densities F_{nI2}, F_{tI2} distributed in the normal and tangential directions along the fictitious boundary for unit cell in body 'I'. However, F_{nI2}, F_{tI2} are not independent and calculated from F_{nM2}, F_{tM2} (see Eq. (11)).

In order to satisfy the boundary conditions for the interface and unit cell, the stress and displacement fields due to ring forces acting in the r- and z-directions in an infinite body will be used. As an example, $h_{nn}^{F_{\mathrm{nM1}}}(r_1, s_1)$ denotes the normal stress induced at the collocation point s_1 when the ring force with unit density $F_{\mathrm{nM1}} = 1$ is acting at the point r_1. Both points s_1 and r_1 are on the fictitious boundary of the inclusion interface. The expression may be found in (Nisitani and Noda, 1984). The notation $\int_{l_1}$ means integrating the ring forces on the boundary for the cylindrical cavity in the body 'M', or the inclusion in the body 'I', and $\int_{l_2}$ means integrating the ring forces on the boundary of the unit cell

$$
\begin{aligned}
&-\frac{1}{2}F_{\mathrm{nM1}}(s_1) - \frac{1}{2}F_{\mathrm{nI1}}(s_1) + \int_{l_1} h_{nn}^{F_{\mathrm{nM1}}}(r_1, s_1)F_{\mathrm{nM1}}(r_1)\mathrm{d}r_1 + \int_{l_1} h_{nn}^{F_{\mathrm{tM1}}}(r_1, s_1)F_{\mathrm{tM1}}(r_1)\mathrm{d}r_1 \\
&- \int_{l_1} h_{nn}^{F_{\mathrm{nI1}}}(r_1, s_1)F_{\mathrm{nI1}}(r_1)\mathrm{d}r_1 - \int_{l_1} h_{nn}^{F_{\mathrm{tI1}}}(r_1, s_1)F_{\mathrm{tI1}}(r_1)\mathrm{d}r_1 + \int_{l_2} h_{nn}^{F_{\mathrm{nM2}}}(r_2, s_1)F_{\mathrm{nM2}}(r_2)\mathrm{d}r_2 \\
&+ \int_{l_2} h_{nn}^{F_{\mathrm{tM2}}}(r_2, s_1)F_{\mathrm{tM2}}(r_2)\mathrm{d}r_2 - \int_{l_2} h_{nn}^{F_{\mathrm{nI2}}}(r_2, s_1)F_{\mathrm{nI2}}(r_2)\mathrm{d}r_2 - \int_{l_2} h_{nn}^{F_{\mathrm{tI2}}}(r_2, s_1)F_{\mathrm{tI2}}(r_2)\mathrm{d}r_2 \\
&= 0
\end{aligned}
\tag{5a}
$$

$$
\begin{aligned}
&-\frac{1}{2}F_{\mathrm{tM1}}(s_1) - \frac{1}{2}F_{\mathrm{tI1}}(s_1) + \int_{l_1} h_{nt}^{F_{\mathrm{nM1}}}(r_1, s_1)F_{\mathrm{nM1}}(r_1)\mathrm{d}r_1 + \int_{l_1} h_{nt}^{F_{\mathrm{tM1}}}(r_1, s_1)F_{\mathrm{tM1}}(r_1)\mathrm{d}r_1 \\
&- \int_{l_1} h_{nt}^{F_{\mathrm{nI1}}}(r_1, s_1)F_{\mathrm{nI1}}(r_1)\mathrm{d}r_1 - \int_{l_1} h_{nt}^{F_{\mathrm{tI1}}}(r_1, s_1)F_{\mathrm{tI1}}(r_1)\mathrm{d}r_1 + \int_{l_2} h_{nt}^{F_{\mathrm{nM2}}}(r_2, s_1)F_{\mathrm{nM2}}(r_2)\mathrm{d}r_2 \\
&+ \int_{l_2} h_{nt}^{F_{\mathrm{tM2}}}(r_2, s_1)F_{\mathrm{tM2}}(r_2)\mathrm{d}r_2 - \int_{l_2} h_{nt}^{F_{\mathrm{nI2}}}(r_2, s_1)F_{\mathrm{nI2}}(r_2)\mathrm{d}r_2 + \int_{l_2} h_{nt}^{F_{\mathrm{tI2}}}(r_2, s_1)F_{\mathrm{tI2}}(r_2)\mathrm{d}r_2 \\
&= 0
\end{aligned}
\tag{5b}
$$

$$\int_{l_1} h_{ur}^{F_{\mathrm{nM1}}}(r_1,s_1)F_{\mathrm{nM1}}(r_1)\mathrm{d}r_1+\int_{l_1} h_{ur}^{F_{\mathrm{tM1}}}(r_1,s_1)F_{\mathrm{tM1}}(r_1)\mathrm{d}r_1-\int_{l_1} h_{ur}^{F_{\mathrm{nI1}}}(r_1,s_1)F_{\mathrm{nI1}}(r_1)\mathrm{d}r_1 -\int_{l_1} h_{ur}^{F_{\mathrm{tI1}}}(r_1,s_1)F_{\mathrm{tI1}}(r_1)\mathrm{d}r_1=0 \tag{5c}$$

$$\int_{l_1} h_{uz}^{F_{\mathrm{nM1}}}(r_1,s_1)F_{\mathrm{nM1}}(r_1)\mathrm{d}r_1+\int_{l_1} h_{uz}^{F_{\mathrm{tM1}}}(r_1,s_1)F_{\mathrm{tM1}}(r_1)\mathrm{d}r_1-\int_{l_1} h_{uz}^{F_{\mathrm{nI1}}}(r_1,s_1)F_{\mathrm{nI1}}(r_1)\mathrm{d}r_1 -\int_{l_1} h_{uz}^{F_{\mathrm{tI1}}}(r_1,s_1)F_{\mathrm{tI1}}(r_1)\mathrm{d}r_1=0 \tag{5d}$$

Eqs. (5a)–(5d) express the boundary conditions along the interface of the inclusion, that is, $\sigma_{\mathrm{nM}}-\sigma_{\mathrm{nI}}=0$, $\tau_{\mathrm{ntM}}-\tau_{\mathrm{ntI}}=0$, $u_{r\mathrm{M}}-u_{r\mathrm{I}}=0$, $u_{z\mathrm{M}}-u_{z\mathrm{I}}=0$. Here, $(u_{r\mathrm{M}},u_{z\mathrm{M}})$ and $(\sigma_{\mathrm{nM}},\tau_{\mathrm{ntM}})$ are the displacements and tractions, respectively, on the fictitious boundary of cylindrical cavities in body 'M'. On the other hand, $(u_{r\mathrm{I}},u_{z\mathrm{I}})$ and $(\sigma_{\mathrm{nI}},\tau_{\mathrm{ntI}})$ are the displacements and tractions, respectively, on the fictitious boundary of cylindrical inclusions in body 'I'.

Similar to Eq. (5), the conditions along the boundary for the unit cell can be expressed by Eq. (7). Here, point P is on the end $z=l_{z2}$, and points Q and Q' are symmetric with respect to the plane $z=l_{z2}/2$ on the surface $r=l_{r2}$ (see Fig. 4). Then,

$$\begin{aligned}&\sigma_0\times\pi l_{r2}^2=\int_0^{l_{r2}}\sigma_z\Big|_{z=l_{z2}}2\pi\,\mathrm{d}r,\\&\tau_{rz}|_{z=l_{z2}}=0,\quad u_z|_{z=l_{z2}}=u_{z0}\quad\text{at } z=l_{z2}\end{aligned} \tag{6}$$

$$\begin{aligned}&0=\int_0^{l_{z2}}\sigma_r\Big|_{z=l_{r2}}2\pi r\,\mathrm{d}r\\&\sigma_r|_{z=z}-\sigma_r|_{z=l_{z2}-z}=0,\quad \tau_{rz}|_{z=z}-\tau_{rz}|_{z=l_{z2}-z}=0\\&u_r|_{z=z}-u_r|_{z=l_{z2}-z}=2u_{r0},\quad u_z|_{z=z}-u_z|_{z=l_{z2}-z}=u_{z0}\\&u_{r0}=\frac{1}{l_{z2}}\int_0^{l_z2}u_r\Big|_{r=l_{r2}}\mathrm{d}z\quad\text{at } r=l_{r2}\end{aligned} \tag{7}$$

By considering an adjacent unit cell as shown in Fig. 4, it is seen that two points $Q(l_{r2},z)$, $Q'(l_{r2},l_{r2}-z)$ should have similar displacement on $r=l_{r2}$. Here, u_{z0} and u_{r0} are still unknown, the following two auxiliary problems will be analyzed instead of solving Fig. 4 directly (Needleman, 1972; Tvergaard, 1981).

Here, an auxiliary problem as shown in Fig. 5(a) has the boundary condition, $u_{z0}=c_1$, $u_{r0}=0$, where c_1 is an arbitrary constant. The other auxiliary problem as shown in Fig. 5(b) has the boundary condition, $u_{r0}=0$, $u_{r0}=c_1$. Under those boundary conditions, the stresses σ_1, σ_2, σ_3, σ_4 will be calculated from Eq. (8). These stresses $\sigma_1\sim\sigma_4$ defined by Eq. (8) will be used to express the problem in Fig. 4 by superposing two auxiliary problems. Here, for example, σ_1 is an average stress σ_z for the auxiliary problem in Fig. 5(a).

$$\begin{aligned}&\sigma_1\times\pi l_{r2}^2=\int_0^{l_{r2}}\sigma_z\Big|_{z=l_{z2}}2\pi r\,\mathrm{d}r\quad\text{at } z=\pm l_{z2}\\&\sigma_2\times 2\pi l_{r2}l_{z2}=\int_{-l_{z2}}^{l_{z2}}\sigma_r\Big|_{r=l_{r2}}2\pi l_{r2}\,\mathrm{d}z\quad\text{at } r=l_{r2}\\&\sigma_3\times\pi l_{r2}^2=\int_0^{l_{r2}}\sigma_z\Big|_{z=l_{z2}}2\pi r\,\mathrm{d}r\quad\text{at } z=\pm l_{z2}\\&\sigma_4\times 2\pi l_{r2}l_{z2}=\int_{-l_{z2}}^{l_{z2}}\sigma_r\Big|_{r=l_{r2}}2\pi l_{r2}\,\mathrm{d}z\quad\text{at } r=l_{r2}\end{aligned} \tag{8}$$

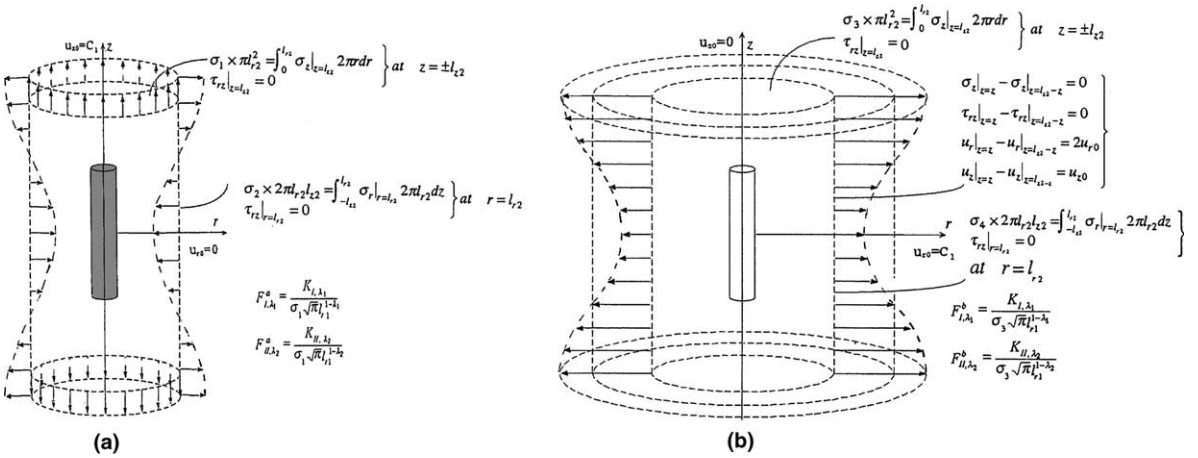

Fig. 5. Auxiliary problems: (a) $u_{r0}=0$, $u_{z0}=c_1$, (b) $u_{r0}=c_1$, $u_{z0}=0$.

Dimensionless stress intensity factors for Figs. 4 and 5(a) and (b) are defined in Eq. (9) having relations (10) (see Appendix A). Here, the eigenvalues λ_1 and λ_2 are given as the roots of eigenequations (3) and (4).

$$\begin{aligned} &F_{\mathrm{I},\lambda_1}=K_{\mathrm{I},\lambda_1}\big/\big(\sigma_0\sqrt{\pi}l_{r1}^{1-\lambda_1}\big), \quad F_{\mathrm{II},\lambda_2}=K_{\mathrm{II},\lambda_2}\big/\big(\sigma_0\sqrt{\pi}l_{r1}^{1-\lambda_2}\big)\\ &F^{a}_{\mathrm{I},\lambda_1}=K_{\mathrm{I},\lambda_1}\big/\big(\sigma_1\sqrt{\pi}l_{r1}^{1-\lambda_1}\big), \quad F^{a}_{\mathrm{II},\lambda_2}=K_{\mathrm{II},\lambda_2}\big/\big(\sigma_1\sqrt{\pi}l_{r1}^{1-\lambda_2}\big)\\ &F^{b}_{\mathrm{I},\lambda_1}=K_{\mathrm{I},\lambda_1}\big/\big(\sigma_3\sqrt{\pi}l_{r1}^{1-\lambda_1}\big), \quad F^{b}_{\mathrm{II},\lambda_2}=K_{\mathrm{II},\lambda_2}\big/\big(\sigma_3\sqrt{\pi}l_{r1}^{1-\lambda_2}\big) \end{aligned} \tag{9}$$

$$F_{\mathrm{I},\lambda_1}=\frac{F^{a}_{\mathrm{I},\lambda_1}-(\sigma_2/\sigma_1)F^{b}_{\mathrm{I},\lambda_1}}{1-(\sigma_2/\sigma_1)(\sigma_3/\sigma_4)}, \quad F_{\mathrm{II},\lambda_2}=\frac{F^{a}_{\mathrm{II},\lambda_2}-(\sigma_2/\sigma_1)F^{b}_{\mathrm{II},\lambda_2}}{1-(\sigma_2/\sigma_1)(\sigma_3/\sigma_4)} \tag{10}$$

In this study, as shown in Eq. (11), the body forces densities, F_{nI2}, F_{tI2} distributed along the fictitious boundary for unit cell are also applied in body 'I' so as to produce the same deformations of body 'M' due to the body forces F_{nM2}, F_{tM2}.

$$\begin{bmatrix} h_{ur}^{F_{\mathrm{nM2}}} & h_{ur}^{F_{\mathrm{tM2}}} \\ h_{uz}^{F_{\mathrm{nM2}}} & h_{uz}^{F_{\mathrm{tM2}}} \end{bmatrix} \cdot \begin{bmatrix} F_{\mathrm{nM2}} \\ F_{\mathrm{tM2}} \end{bmatrix} = \begin{bmatrix} h_{ur}^{F_{\mathrm{nI2}}} & h_{ur}^{F_{\mathrm{tI2}}} \\ h_{uz}^{F_{\mathrm{nI2}}} & h_{uz}^{F_{\mathrm{tI2}}} \end{bmatrix} \cdot \begin{bmatrix} F_{\mathrm{nI2}} \\ F_{\mathrm{tI2}} \end{bmatrix} \tag{11}$$

Since the relation (11) is satisfied, Eqs. (5c), (5d) does not include the integral involving the term $h_{ur}^{F_{\mathrm{nM2}}}(r_2,s_1)$ etc.

3. Numerical solutions of singular integral equations

Numerical solutions will be explained by taking an example for the boundary conditions for corner A. Fig. 6 illustrates boundary divisions for the solutions of Eqs. (1)–(3) when $l_{z1}/l_{r1}=10$, $l_{z2}/l_{z1}=2$, $l_{r2}/l_{r1}=5$. It should be noted that the body forces, F_{n} and F_{t} (see Fig. 4(b)), acting in the normal and tangential directions, should be expressed as a combination of symmetric mode I type $r_1^{\lambda_1-1}$ and skew-symmetric mode II type $r_1^{\lambda_2-1}$ to the bisector of the corners (Chen, 1992). Here, r_1 is a distance measured from the corner A. The body force densities distributed in the regions A′2–A–A2 is expressed as follows using fundamental densities $r_1^{\lambda_1-1}$, $r_1^{\lambda_2-1}$ and weight functions $W^{\mathrm{I}}_{\mathrm{nM1}}\sim W^{\mathrm{II}}_{\mathrm{tM1}}$.

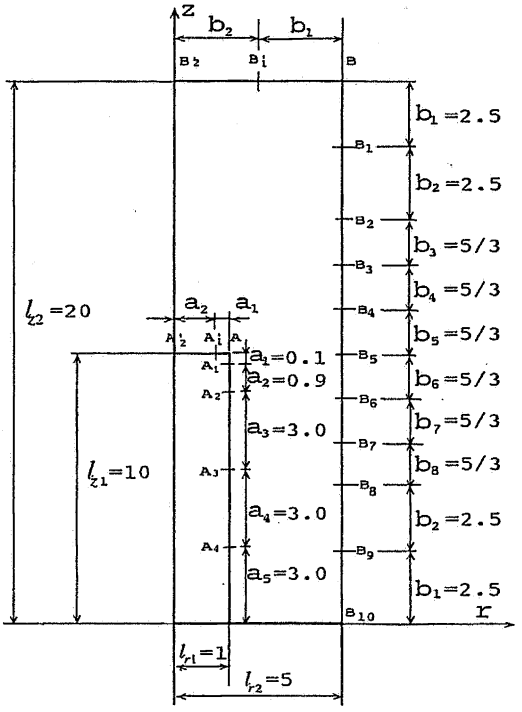

Fig. 6. Boundary division when $l_{z1}/l_{r1} = 10$, $l_{r2}/l_{r1} = 5$, $l_{z2}/l_{z1} = 2$.

$$
\begin{aligned}
F_{\mathrm{nM1}}(r_1) &= F^{\mathrm{I}}_{\mathrm{nM1}}(r_1) + F^{\mathrm{II}}_{\mathrm{nM1}}(r_1) = W^{\mathrm{I}}_{\mathrm{nM1}}(r_1) r_1^{\lambda_1 - 1} + W^{\mathrm{II}}_{\mathrm{nM1}}(r_1) r_1^{\lambda_2 - 1} \\
F_{\mathrm{tM1}}(r_1) &= F^{\mathrm{I}}_{\mathrm{tM1}}(r_1) + F^{\mathrm{II}}_{\mathrm{tM1}}(r_1) = W^{\mathrm{I}}_{\mathrm{tM1}}(r_1) r_1^{\lambda_1 - 1} + W^{\mathrm{II}}_{\mathrm{tM1}}(r_1) r_1^{\lambda_2 - 1} \\
F_{\mathrm{nI1}}(r_1) &= F^{\mathrm{I}}_{\mathrm{nI1}}(r_1) + F^{\mathrm{II}}_{\mathrm{nI1}}(r_1) = W^{\mathrm{I}}_{\mathrm{nI1}}(r_1) r_1^{\lambda_1 - 1} + W^{\mathrm{II}}_{\mathrm{nI1}}(r_1) r_1^{\lambda_2 - 1} \\
F_{\mathrm{tI1}}(r_1) &= F^{\mathrm{I}}_{\mathrm{tI1}}(r_1) + F^{\mathrm{II}}_{\mathrm{tI1}}(r_1) = W^{\mathrm{I}}_{\mathrm{tI1}}(r_1) r_1^{\lambda_1 - 1} + W^{\mathrm{II}}_{\mathrm{tI1}}(r_1) r_1^{\lambda_2 - 1}
\end{aligned}
\tag{12}
$$

$$
\begin{aligned}
W^{\mathrm{I}}_{\mathrm{nM1}}(r_1) &= \sum_{n=1}^{M} a_n r_1^{n-1}, \quad W^{\mathrm{I}}_{\mathrm{tM1}}(r_1) = \sum_{n=1}^{M} b_n r_1^{n-1} \\
W^{\mathrm{II}}_{\mathrm{nM1}}(r_1) &= \sum_{n=1}^{M} c_n r_1^{n-1}, \quad W^{\mathrm{II}}_{\mathrm{tM1}}(r_1) = \sum_{n=1}^{M} d_n r_1^{n-1} \\
W^{\mathrm{I}}_{\mathrm{nI1}}(r_1) &= \sum_{n=1}^{M} e_n r_1^{n-1}, \quad W^{\mathrm{I}}_{\mathrm{tI1}}(r_1) = \sum_{n=1}^{M} f_n r_1^{n-1} \\
W^{\mathrm{II}}_{\mathrm{nI1}}(r_1) &= \sum_{n=1}^{M} g_n r_1^{n-1}, \quad W^{\mathrm{II}}_{\mathrm{tI1}}(r_1) = \sum_{n=1}^{M} h_n r_1^{n-1}
\end{aligned}
\tag{13}
$$

Eqs. (12) and (13) do not include the terms expressing local uniform stretching and shear distortion at the corner A. Therefore the body forces densities are applied also in the body 'I' in order to express local uniform stretching and shear distortion at the corner A (see Eq. (11)).

On the numerical solution as shown in Eqs. (12), (13), the singular integral equations (5)–(7) are reduced to algebraic equations for the determination of the unknown coefficients $a_{\mathrm{n}} \sim h_{\mathrm{n}}$. These coefficients are determined from the boundary conditions at suitably chosen collocation points. The generalized stress

intensity factors K_{I,λ_1}, $K_{\mathrm{II},\lambda_2}$ for angular corners can be obtained from the values of $W_{\mathrm{n}}^{\mathrm{I}}(0), W_{\mathrm{n}}^{\mathrm{II}}(0), W_{\mathrm{t}}^{\mathrm{I}}(0), W_{\mathrm{t}}^{\mathrm{II}}(0)$ at the corner tip (Noda et al., 1996).

4. Results and discussion

4.1. Convergence of the results

In the following calculations Poisson's ratio is assumed as $\nu_{\mathrm{I}} = \nu_{\mathrm{M}} = 0.3$. Generalized stress intensity factors $K_{1,\lambda 1}$, $K_{\mathrm{II},\lambda 2}$ are analyzed with varying dimensions of inclusion and unit cell, and elastic ratio $G_{\mathrm{I}}/G_{\mathrm{M}}$.

Table 1
Convergence of F_{I,λ_1} and $F_{\mathrm{II},\lambda_2}$ for (a) periodic array when $l_{z1}/l_{r1} = 10$, $l_{z2}/l_{z1} = 5$, $l_{r2}/l_{r1} = 20$; (b) zigzag array when $l_{z1}/l_{r1} = 30$, $l_{z2}/l_{r1} = 31$, $l_{r2}/l_{r1} = 2.2$

M	$F_{\mathrm{I},\lambda 1}$	$F_{\mathrm{II},\lambda 2}$	$F_{\mathrm{I},\lambda 1}$	$F_{\mathrm{II},\lambda 2}$
(a)				
	$G_{\mathrm{I}}/G_{\mathrm{M}} = 10^2$		$G_{\mathrm{I}}/G_{\mathrm{M}} = 10^{-5}$	
3	1.2871	1.7952	0.3786	1.5998
4	1.2898	1.7989	0.3789	1.6042
5	1.2903	1.7993	0.3790	1.6051
6	1.2900	1.7988	0.3787	1.6055
(b)				
	$G_{\mathrm{I}}/G_{\mathrm{M}} = 60$		$G_{\mathrm{I}}/G_{\mathrm{M}} = 10^2$	
3	0.4398	0.5354	0.4588	0.4872
4	0.4407	0.5368	0.4613	0.4921
5	0.4416	0.5375	0.4628	0.4925
6	0.4413	0.5371	0.4628	0.4924

Table 2
Mechanical properties of (a) carbon fiber-reinforced plastics and (b) glass fiber-reinforced plastics

	Polycarbonate/carbon fiber	Polyamid/carbon fiber	Polyphenylene sulfide/carbon fiber
(a)			
Young's modulus of matrix (MPa)	2000	2800	3800
Density of matrix (g/cm^3)	1.19–1.23	1.14–1.16	1.35
Young's modulus of fiber (MPa)	235,000	235,000	235,000
Density of fiber (g/cm^3)	1.80	1.80	1.80
Aspect ratio of fiber (average)	30	30	30
Elastic ratio $G_{\mathrm{I}}/G_{\mathrm{M}}$	118	84	61
Weight percent of fiber (%)	30	30	30
Volume percent of fiber (%)	22.08–22.68	21.37–21.65	24.30
(b)			
	Polypropylene/glass fiber	Polyethylene/glass fiber	Polyethylene/glass fiber
Young's modulus of matrix (MPa)	900–1300	950–1400	3100–3200
Density of matrix (g/cm^3)	0.89–0.91	0.94–0.96	1.04–1.05
Young's modulus of fiber (MPa)	76,000	76,000	76,000
Density of fiber (g/cm^3)	2.51	2.51	2.51
Aspect ratio of fiber (average)	30	30	30
Elastic ratio $G_{\mathrm{I}}/G_{\mathrm{M}}$	58–84	54–80	24–25
Weight percent of fiber (%)	40	40	40
Volume percent of fiber (%)	19.09–19.44	19.96–20.29	21.62–21.79

Table 3
(a) F_{I,λ_1} and (b) $F_{\mathrm{II},\lambda_2}$ for periodic and zigzag arrays when $G_\mathrm{I}/G_\mathrm{M} = 60$, $l_{z1}/l_{r1} = 30$

Volume percent of fiber (%)	Case 1			Case 2			Case 3		
	Zigzag array	Periodic array	l_{z2}/l_{r2}	Zigzag array	Periodic array	l_{z2}/l_{r2}	Zigzag array	Periodic array	l_{z2}/l_{r2}
(a)									
25	0.411	0.391	15.78	0.624	0.384	17.71	0.113	0.358	20.58
20	0.441	0.435	14.09	0.706	0.424	19.61	0.119	0.393	25.72
15	0.506	0.489	12.18	0.821	0.451	20.37	0.127	0.338	34.30
5	0.855	0.801	7.02	1.125	0.776	48.13	0.563	0.713	103.11
$\to 0$	1.556	1.556	–	1.556	1.556	–	1.556	1.556	–
(b)									
25	0.450	0.399	15.78	0.788	0.386	17.81	0.310	0.365	20.58
20	0.537	0.503	14.09	0.972	0.479	19.66	0.376	0.435	25.72
15	0.650	0.586	12.18	1.043	0.559	21.27	0.400	0.431	34.30
5	1.249	1.194	7.02	1.493	1.176	46.32	1.052	1.132	103.11
$\to 0$	2.156	2.156	–	2.156	2.156	–	2.156	2.156	–

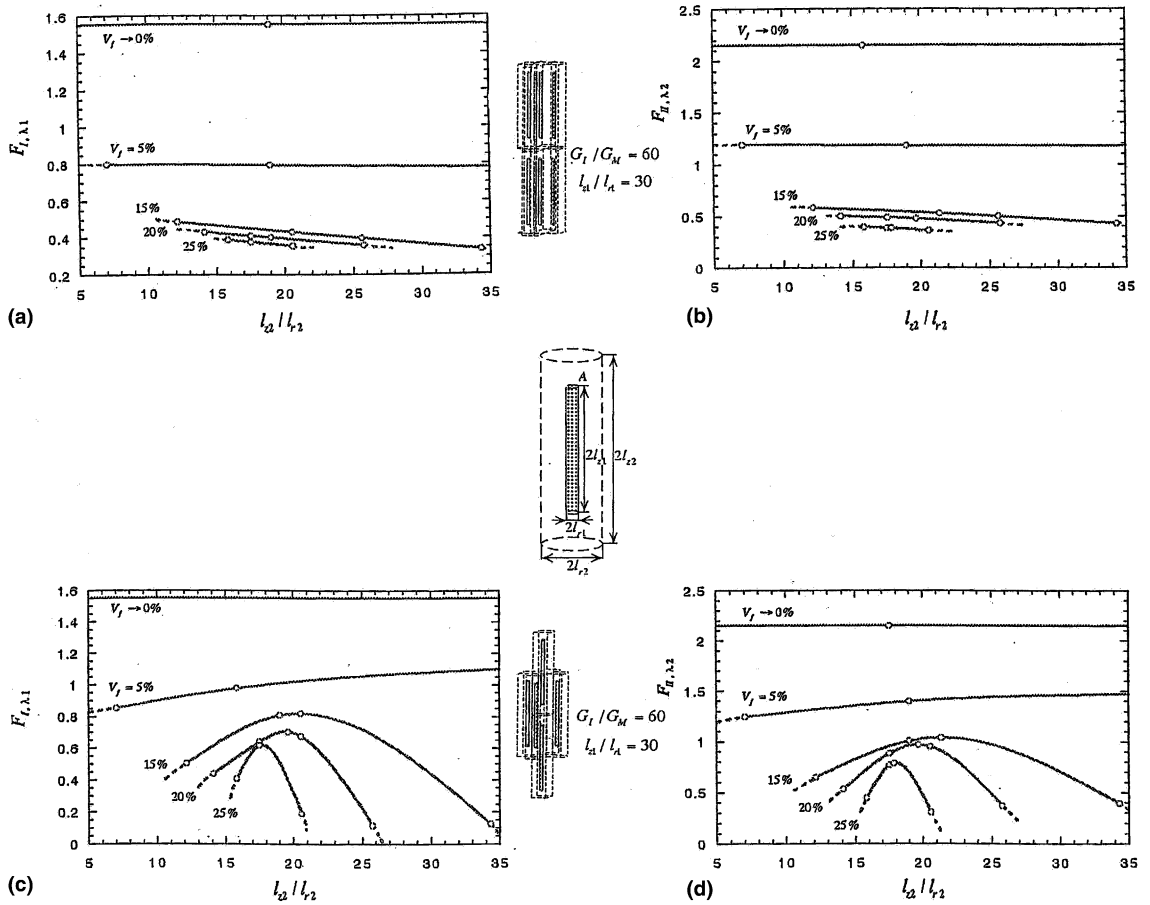

Fig. 7. (a) F_{I,λ_1}, (b) $F_{\mathrm{II},\lambda_2}$ for periodic array, (c) F_{I,λ_1}, (d) $F_{\mathrm{II},\lambda_2}$ for zigzag array when $G_1/G_\mathrm{M} = 60$, $l_{z1}/l_{r1} = 30$.

Some examples of convergence are shown in Table 1 when $l_{z1}/l_{r1} = 10$, $l_{z2}/l_{z1} = 2$, $l_{r2}/l_{r1} = 5$. Since the results obtained from $W_{\mathrm{n}}^{\mathrm{I}}(0)$ and $W_{\mathrm{t}}^{\mathrm{I}}(0)$, have a few percent differences, the average values are indicated (Noda et al., 2000, 2003). The results have good convergence to the forth digit when $M = 4$–6, where M is a number of collocation points at each division of boundaries. In the following calculation the generalized stress intensity factors (GSIF) are shown confirming the convergence as shown in Table 1.

4.2. Effect of volume fraction and elastic modulus ratio on the GSIF

In this study, periodic and zigzag arrays of cylindrical inclusions will be analyzed. Then, parametric studies will be conducted to address the issue of optimal arrangement of cylindrical inclusions given the same volume fraction and material properties. Table 2 shows the mechanical properties of short fiber-reinforced plastics. As shown in these tables, in most cases, the aspect ratio of fiber is 30; in the following calculation, therefore, fiber's aspect ratio is fixed as $l_{z1}/l_{r1} = 30$. In Table 3 and Fig. 7, the elastic modulus ratio is fixed

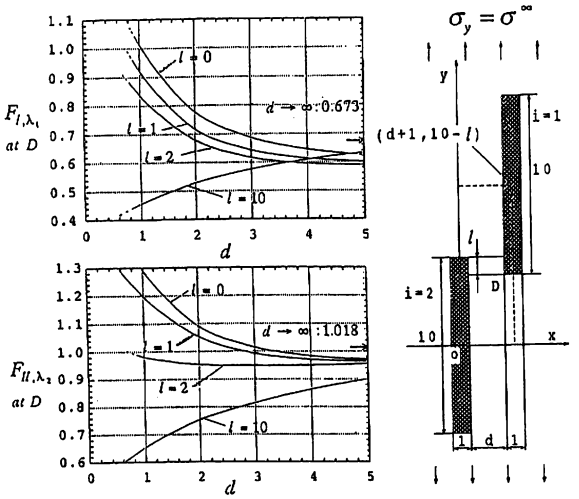

Fig. 8. Results for two rectangular inclusions under plane strain when $G_{\mathrm{I}}/G_{\mathrm{M}} = 100$, $\nu_{\mathrm{I}} = \nu_{\mathrm{M}} = 0.3$: (a) F_{I,λ_1} at D vs. d relation (b) $F_{\mathrm{II},\lambda_2}$ at D vs. d relation.

Table 4
(a) F_{I,λ_1} and (b) $F_{\mathrm{II},\lambda_2}$ for periodic and zigzag arrays when volume percent of fiber $V_f = 20\%$, $l_{z1}/l_{r1} = 30$

$G_{\mathrm{I}}/G_{\mathrm{M}}$	Case 1			Case 2			Case 3			$V \to 0\%$
	Zigzag array	Periodic array	l_{z2}/l_{r2}	Zigzag array	Periodic array	l_{z2}/l_{r2}	Zigzag array	Periodic array	l_{z2}/l_{r2}	
(a)										
10	0.368	0.363	14.09	0.609	0.337	18.43	0.105	0.270	25.72	0.617
60	0.441	0.435	14.09	0.693	0.404	19.31	0.119	0.361	25.72	1.556
100	0.463	0.440	14.09	0.740	0.382	19.58	0.111	0.305	25.72	1.943
(b)										
10	0.582	0.567	14.09	1.038	0.507	20.50	0.402	0.453	25.72	1.124
60	0.537	0.503	14.09	0.967	0.470	19.81	0.435	0.435	25.72	2.156
100	0.492	0.476	14.09	0.850	0.429	18.77	0.356	0.356	25.72	2.673

as $G_I/G_M = 60$, then the effect of volume fraction V_f of fibers is considered. As shown in Fig. 7, for both periodic and zigzag arrays, the F_{I,λ_1} and F_{II,λ_2} decrease with increasing V_f. As shown in Fig. 7, for periodic array, the F_{I,λ_1} and F_{II,λ_2} decrease with increasing l_{z2}/l_{r2}. On the other hand, for zigzag array, the F_{I,λ_1} and F_{II,λ_2} have peak values at a certain value of l_{z2}/l_{r2} as shown in Fig. 7.

The reason for appearing peak values in zigzag array in Fig. 7 can be explained from the results of two rectangular inclusions in matrix as shown in Fig. 8 (Noda et al., 2000). With decreasing the distance d, the F_{I,λ_1} and F_{II,λ_2} values decrease if two inclusions are in the transverse direction (see $l = 10$ in Fig. 8). On the other hand, if two inclusions are in the oblique direction, the F_{I,λ_1} and F_{II,λ_2} values increase with decreasing the distance d (see $l = 0$, 1, 2 in Fig. 8). With decreasing d in a zigzag array, two types of inclusions, which have different interaction which have different effects of interaction, approach each other; one is in the transverse direction, the other in the in the oblique directions. Therefore, at a certain distance the interaction may be larger.

From the parametric studies for zigzag and periodic arrays, it may be concluded that large aspect ratio of unit cell l_{z2}/l_{r2} may be desirable for short fiber-reinforce composites because the singular stress is not larger unless adjacent fibers are very close or touch.

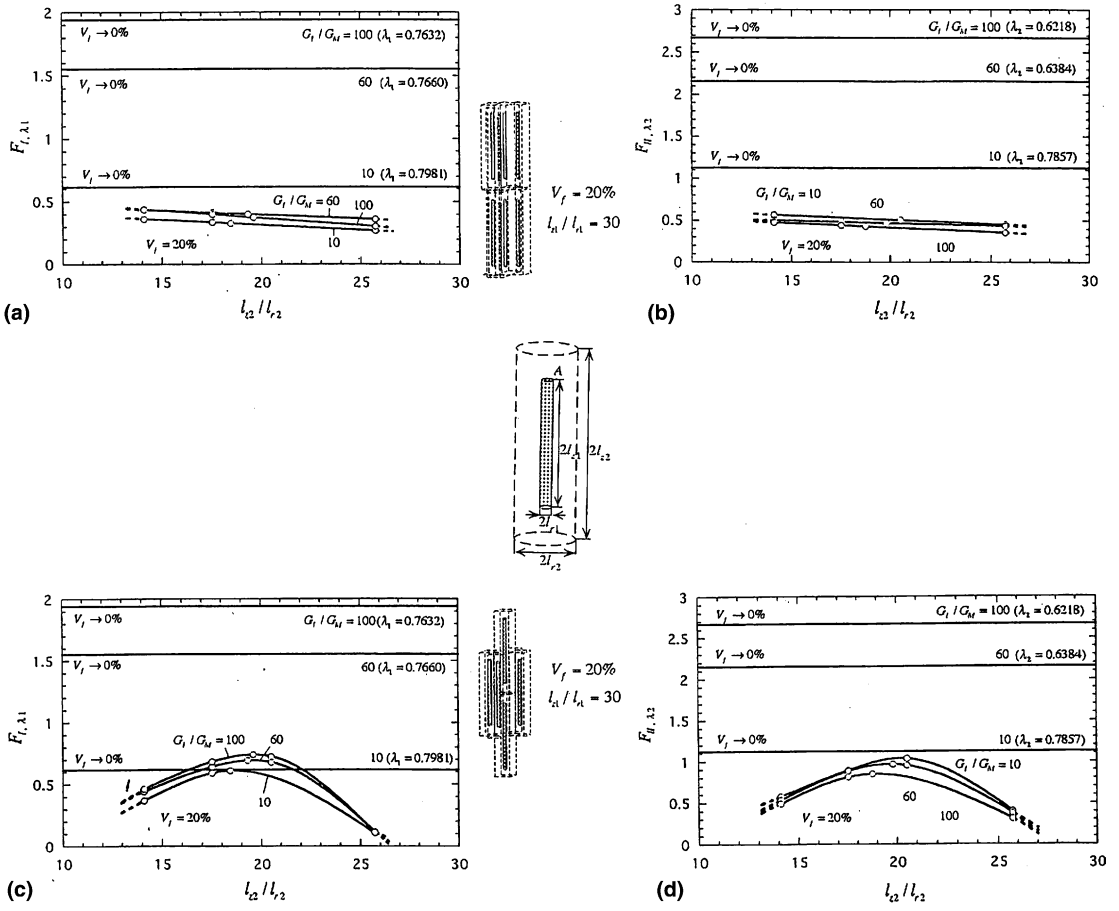

Fig. 9. (a) F_{I,λ_1}, (b) F_{II,λ_2} for periodic array, (c) F_{I,λ_1}, (d) F_{II,λ_2} for zigzag array when $V_f = 20\%$, $l_{z1}/l_{r1} = 30$.

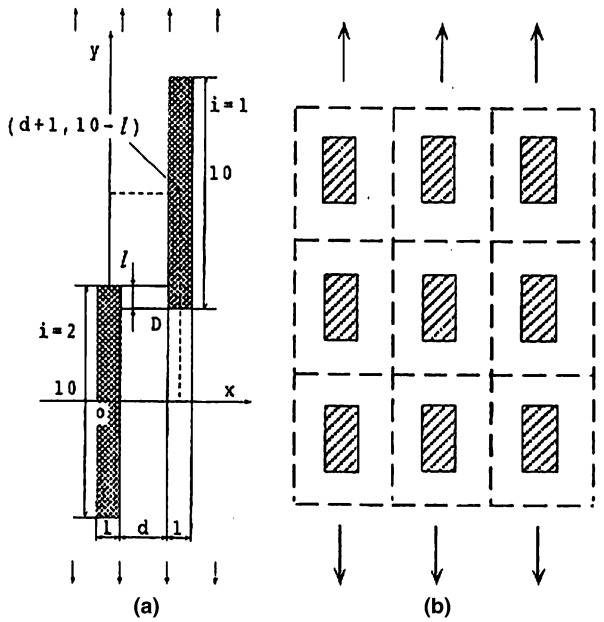

Fig. 10. Two-dimensional models: (a) two rectangular inclusions and (b) a periodic array of rectangular inclusions.

Table 5
F_{I,λ_1} and $F_{\mathrm{II},\lambda_2}$ for (a) periodic array of rectangular inclusions in Fig. 6(b) and (b) periodic array of cylindrical inclusions in Fig. 3 when $G_{\mathrm{I}}/G_{\mathrm{M}} = 10^2$, $l_{z1}/l_{r1} = 10$

l_{r2}/l_{r1}	l_{z2}/l_{z1}					
	$F_{\mathrm{I},\lambda 1}$ ($\lambda_1 = 0.76323491$)			$F_{\mathrm{II},\lambda 2}$ ($\lambda_2 = 0.62184397$)		
	2	5	10	2	5	10
(a)						
5	0.486	0.472	0.470	0.706	0.775	0.806
10	0.609	0.603	0.602	0.925	0.967	0.983
20	0.672	0.656	0.655	1.038	*1.016*	*1.026*
30	0.702	*0.666*	*0.665*	1.086	*1.018*	*1.023*
50	0.731	*0.672*	*0.670*	1.131	*1.019*	*1.019*
(b)						
	1.5	2	5	1.5	2	5
5	0.935	0.942	0.953	1.247	1.284	1.357
10	1.238	1.229	1.233	1.725	1.708	1.731
15	1.309	1.281	1.280	1.832	1.784	*1.788*
20	1.328	1.298	*1.290*	1.869	1.810	*1.799*
25	1.347	1.303	*1.294*	1.890	1.813	*1.802*
30	1.359	1.309	*1.295*	1.904	1.816	*1.803*
50	–	1.314	*1.295*	–	1.820	*1.803*

For (a): $F_{\mathrm{I},\lambda 1} \to 0.671$, $F_{\mathrm{II},\lambda 2} \to 1.018$ if $l_{r2}/l_{r1} \to \infty$ $l_{z2}/l_{z1} \to \infty$.
For (b): $F_{\mathrm{I},\lambda 1} \to 1.297$, $F_{\mathrm{II},\lambda 2} \to 1.804$ if $l_{r2}/l_{r1} \to \infty$ $l_{z2}/l_{z1} \to \infty$.
Region within 1% interaction are in italics.

In Table 4 and Fig. 9, the volume fraction is fixed as $V_f = 0$ and 20%, then the effect of elastic ratio G_I/G_M is considered. As shown in Tables 2 and 3, $V_f = 20\%$ corresponds to most cases of the reinforced plastics. In Fig. 9, each curve corresponds to the distinct singularity index λ_1, λ_2. With increasing the elastic ratio' as $G_I/G_M = 10 \to 100$, the interaction becomes larger under the same geometrical condition. For example, when $G_I/G_M = 100$, as shown in Fig. 9, $F_{I,\lambda_1}/F_{I,\lambda_1}|_{v_f\to 0} = 0.06$–$0.38$, $F_{II,\lambda 2}/F_{II,\lambda 2}|_{V_f\to 0} = 0.13$–$0.32$. On the other hand, when $G_I/G_M = 10$, $F_{I,\lambda 1}/F_{I,\lambda 1}|_{V_f\to 0} = 0.17$–$0.99$, $F_{II,\lambda 2}/F_{II,\lambda 2}|_{V_f\to 0} = 0.36$–$0.92$. From the results of zigzag arrays in Fig. 9, it should be noted that F_{I,λ_1} and F_{II,λ_2} have largest values at $l_{z2}/l_{r2} \cong 20$ when $V_f = 20\%$ almost independent of G_I/G_M.

4.3. Comparison between 3D arrays and 2D arrays

In the previous studies the interaction between two rectangular inclusions as shown in Fig. 10(a) have been treated as a two-dimensional models of fibers (Noda et al., 1998, 2000). Since it is very difficult to deal with the three-dimensional problem of Fig. 10(a), it is important to discuss the difference between the results of two- and three-dimensional modeling. In Table 5 and Fig. 11, the results of a periodic array of cylindrical inclusions are compared with the ones of a periodic array of rectangular inclusions when $G_I/G_M = 10^2$ and $l_{z1}/l_{r1} = 10$. In this case, if the size of unit cell is larger enough, the results coincide with the ones of a single inclusion, that is, $F_{I,\lambda_1} \to 1.297$ and $F_{II,\lambda_2} \to 1.804$ for a cylindrical inclusion, and $F_{I,\lambda_1} \to 0.671$ and $F_{I,\lambda_1} \to 1.018$ for a rectangular inclusion. In Fig. 11, first, consider the case of $l_{r2}/l_{r1} = 50$ and $l_{z2}/l_{z1} = 2$, where the distance in the r-direction is large enough. Because of the interaction of fibers in the z-direction, the F_{I,λ_1} is larger than the case of $l_{z2}/l_{z1} \to \infty$ by 9% for rectangular inclusions, and by 1% for cylindrical inclusions. In other words, the effect of distance l_{z2} is smaller in 3D arrays than in 2D arrays. Next, assume the distance in the z-direction is large enough, for example, $l_{z2}/l_{z1} = 5$. Then, it is found that if $l_{r2}/l_{r1} \geqslant 30$ the effect of interaction on F_{I,λ_1} is less than 1% for 2D inclusions. On the other hand, if $l_{z2}/l_{z1} = 5$ and $l_{r2}/l_{r1} \geqslant 20$ for cylindrical inclusions, the effect of interaction on is less than 1%.

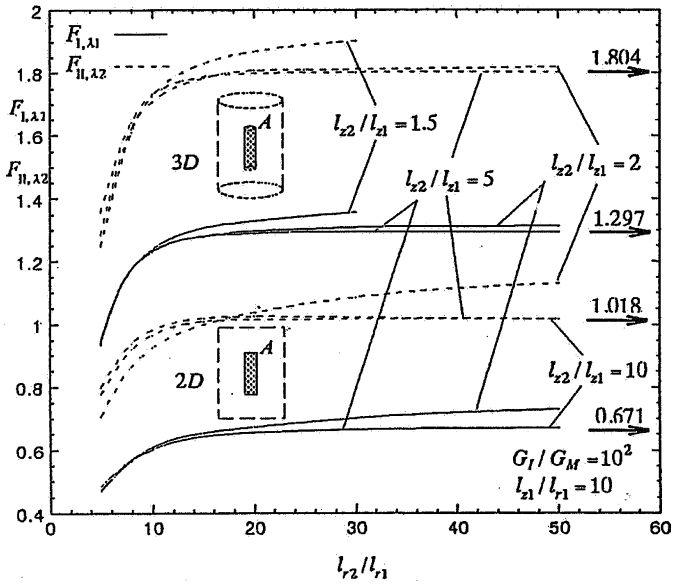

Fig. 11. Comparison between rectangular inclusion and cylindrical inclusions.

The effect of the distance in the r-direction in 3D arrays is also smaller than in 2D arrays. The region is indicated by a solid line in Table 5.

4.4. The region within 1% interaction

In this section, spacing of fibers when the interaction can be negligible will be considered assuming periodic arrangement. Table 6(a) shows the results when $G_I/G_M = 10^2$ and $l_{z1}/l_{r1} = 5$. From Table 6(a), it is seen that if $l_{r2}/l_{r1} \geqslant 5$ for $l_{z1}/l_{r1} = 2$ the interaction on F_{I,λ_1} is less than 1%. Also, if $l_{r2}/l_{r1} \geqslant 50$ for $l_{z1}/l_{r1} = 30$, the interaction on F_{I,λ_1} is less than 1%. That means, with increasing the fiber length, the interaction becomes larger. Similarly, Table 6(b) shows the results when $G_I/G_M = 10$ and $l_{z1}/l_{r1} = 2$. When $l_{z1}/l_{r1} = 10$, $l_{r2}/l_{r1} = 5$ for $G_I/G_M = 10$, F_{I,λ_1} decreases by 11%. Under the same geometrical condition, F_{I,λ_1} decreases by 27% for $G_I/G_M = 10^2$. In other words, with increasing the elastic ratio G_I/G_M, the effect of interaction becomes larger. Similar tendency can been seen in Table 3(c) for $G_I/G_M = 2$ with $l_{z2}/l_{z1} = 2$.

Table 6
F_{I,λ_1} and F_{II,λ_2} for periodic array of cylindrical inclusions in Fig. 3. (a) $G_I/G_M = 10^2$ and $l_{z1}/l_{r1} = 10$ (b) $G_I/G_M = 10$ and $l_{z1}/l_{r1} = 2$ (c) $G_I/G_M = 2$ and l_{z2}/l_{z1}

(a) l_{r2}/l_{r1}	l_{z1}/l_{r1}							
	$F_{I,\lambda 1}$ ($\lambda_1 = 0.76323491$)				$F_{II,\lambda 2}$ ($\lambda_2 = 0.62184397$)			
	2	10	20	30	2	10	20	30
3	0.451	–	–	–	0.725	–	–	–
5	*0.485*	0.953	0.973	1.055	*0.755*	1.357	1.365	1.381
10	*0.493*	1.233	1.493	1.529	*0.757*	1.730	2.073	2.117
20	*0.496*	*1.290*	1.709	1.849	*0.760*	*1.799*	2.363	2.549
30	*0.497*	*1.295*	*1.738*	1.910	*0.761*	*1.803*	*2.399*	2.631
50	*0.497*	*1.295*	*1.746*	*1.930*	*0.761*	*1.804*	*2.407*	*2.660*
∞	*0.495*	*1.297*	*1.753*	*1.943*	*0.759*	*1.804*	*2.416*	*2.673*

(b) l_{r2}/l_{r1}	l_{z1}/l_{r1}					
	$F_{I,\lambda 1}$ ($\lambda_1 = 0.79811118$)			$F_{II,\lambda 2}$ ($\lambda_2 = 0.78565474$)		
	5	10	100	5	10	100
5	0.510	0.553	–	0.936	0.963	–
10	*0.538*	0.584	0.585	*0.996*	1.063	1.061
15	*0.539*	*0.594*	0.602	*0.997*	*1.083*	1.095
20	*0.540*	*0.596*	0.608	*0.997*	*1.089*	1.107
30	*0.541*	*0.598*	*0.612*	*0.998*	*1.087*	*1.115*
50	–	*0.599*	*0.616*	–	*1.089*	*1.121*
∞	*0.540*	*0.599*	*0.618*	*0.996*	*1.087*	*1.121*

(c) l_{r2}/l_{r1}	l_{z1}/l_{r1}							
	$F_{I,\lambda 1}$ ($\lambda_1 = 0.91091019$)				$F_{II,\lambda 2}$ ($\lambda_2 = 0.9810170$)			
	10	30	60	100	10	30	60	100
5	0.250	0.250	0.251	0.250	3.235	3.238	3.239	3.240
10	*0.253*	*0.254*	0.252	0.251	*3.282*	*3.282*	3.271	3.242
15	*0.253*	*0.254*	*0.255*	0.252	*3.288*	*3.289*	*3.288*	3.273
20	*0.254*	*0.254*	*0.255*	*0.253*	*3.291*	*3.291*	*3.290*	*3.287*
30	*0.255*	*0.255*	*0.255*	*0.254*	*3.295*	*3.298*	*3.298*	*3.296*
50	*0.255*	*0.255*	*0.255*	*0.255*	*3.299*	*3.301*	*3.301*	*3.300*

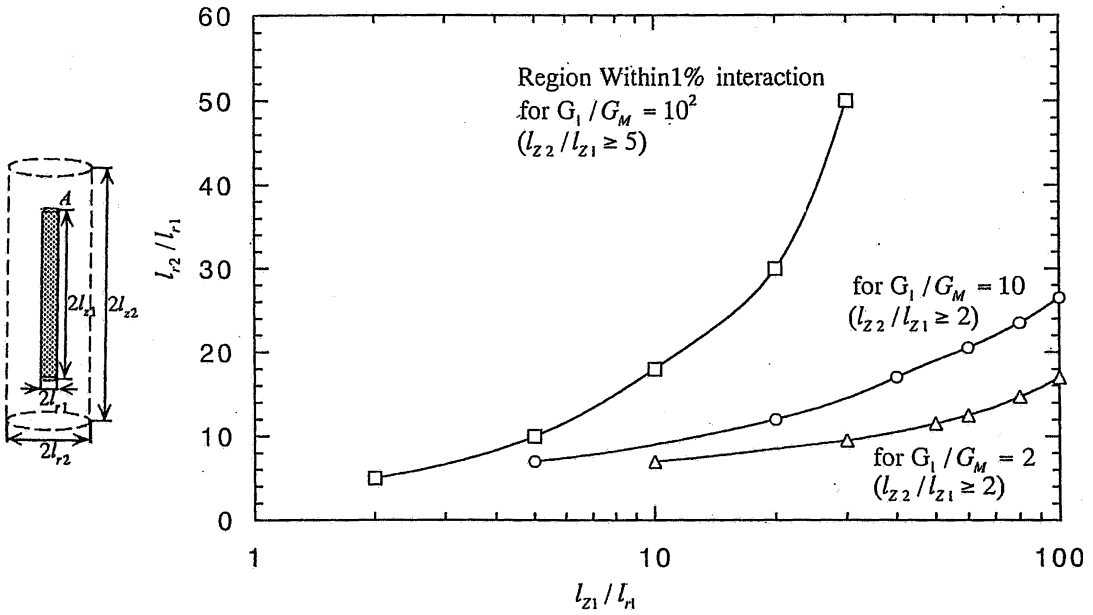

Fig. 12. Region within 1% interaction.

Fig. 12 shows the region of l_{r2}/l_{r1}, where the interaction is less than 1%, as a function of l_{z2}/l_{z1}. As shown in Fig. 12, with increasing l_{z2}/l_{z1}, the larger distance l_{r2}/l_{r1} is necessary for less than 1% interaction.

Regarding the region of l_{z2}/l_{z1}, we can see the following. When $G_I/G_M = 10^2$, $l_{z2}/l_{z1} \geqslant 5$ is necessary for less than 1% interaction. Also, when $G_I/G_M \leqslant 10$, $l_{z2}/l_{z1} \geqslant 2$ is necessary for less than 1% interaction.

5. Conclusion

To evaluate the mechanical strength of fiber-reinforced composites it is necessary to evaluate singular stresses at the end of fibers. In this paper, therefore, periodic and zigzag arrays of cylindrical inclusions in matrix under longitudinal tension are analyzed by the application of the body force method. The conclusions can be made in the following way.

(1) Generalized stress intensity factors at the fiber end are systematically calculated and shown in Figures and Tables with varying the elastic ratio, length, and spacing of fibers. The interaction becomes larger with increasing fiber length and elastic ratio. The region when the interaction effect is less than 1% is shown in figure as a function of fiber length.

(2) As shown in Fig. 12, for both periodic and zigzag arrays, the F_{I,λ_1} and F_{II,λ_2} decrease with increasing V_f. For periodic array, the F_{I,λ_1} and F_{II,λ_2} decrease with increasing the aspect ratio of the unit cell. On the other hand, for zigzag array, the F_{I,λ_1} and F_{II,λ_2} have peak values at a certain value of as shown in Fig. 12.

(3) From the parametric studies for zigzag and periodic arrays, it may be concluded that large aspect ratio of unit cell l_{z2}/l_{r2} may be desirable for short fiber-reinforce composites because the singular stress is not larger unless adjacent fibers are very close or touch. From the results of zigzag arrays in Fig. 9,

it should be noted that F_{I,λ_1} and $F_{\mathrm{II},\lambda_2}$ have the largest values at $l_{z2}/l_{r2} \cong 20$ when $V_f = 20\%$ almost independent of $G_{\mathrm{I}}/G_{\mathrm{M}}$. With increasing the elastic ratio as $G_{\mathrm{I}}/G_{\mathrm{M}} = 10$–$100$, the interaction becomes larger under the same geometrical condition as shown in Fig. 8.

Acknowledgements

The authors wish to express their thanks to the member of their group, especially Mr. T. Iizuka and Mr. N. Ishii, who carried out much of the constructional work.

Appendix A. Relation between the results of given and auxiliary problems

In this study two auxiliary problems were analyzed instead of solving Fig. 4 directly. The final results were given by Eq. (10), which can be derived in the following way. The boundary conditions of the given problem as shown in Fig. A.1(a) are $\sigma_{z\mathrm{av}} = \sigma_0$, $\sigma_{r\mathrm{av}} = 0$, and the results are $F^a_{\mathrm{I},\lambda_1}, F^a_{\mathrm{II},\lambda_2}$. Here $\sigma_{z\mathrm{av}}$ is an average stress at $z = \pm l_{z2}$, and $\sigma_{r\mathrm{av}}$ is an average stress at $r = l_{r2}$. On the other hand, the boundary conditions in Fig. A.1(b) are $\sigma_{z\mathrm{av}} = 0$, $\sigma_{r\mathrm{av}} = \sigma'_0$, and the results are $F^b_{\mathrm{I},\lambda_1}$, $F^b_{\mathrm{II},\lambda_2}$. Under this situation, the dimensionless stress intensity factors, for auxiliary problems as shown in Fig. A.2 can be expressed as follows:

$$F^a_{\mathrm{I},\lambda_1} = F_{\mathrm{I},\lambda_1} + \frac{\sigma_2}{\sigma_1} F'_{\mathrm{I},\lambda_1}, \quad F^b_{\mathrm{I},\lambda_1} = F'_{\mathrm{I},\lambda_1} + \frac{\sigma_3}{\sigma_4} F_{\mathrm{I},\lambda_1} \tag{A.1}$$

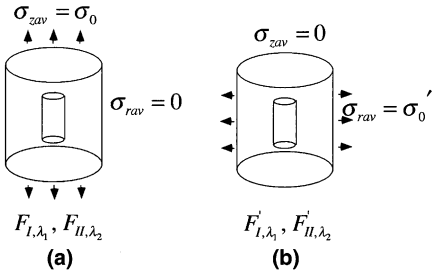

Fig. A.1. Problems to be solved (a), (b).

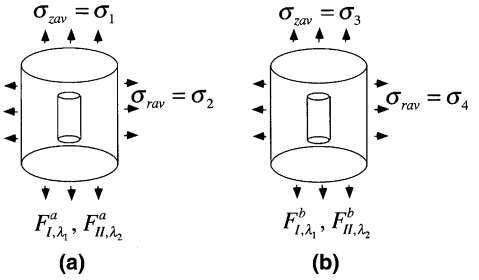

Fig. A.2. Auxiliary problems (a), (b).

$$F^{a}_{\mathrm{II},\lambda_2} = F_{\mathrm{II},\lambda_2} + \frac{\sigma_2}{\sigma_1} F'_{\mathrm{II},\lambda_2}, \quad F^{b}_{\mathrm{II},\lambda_2} = F'_{\mathrm{II},\lambda_2} + \frac{\sigma_3}{\sigma_4} F_{\mathrm{II},\lambda_2} \tag{A.2}$$

From these equations, we have

$$F_{\mathrm{I},\lambda_1} = \frac{F^{a}_{\mathrm{I},\lambda_1} - (\sigma_2/\sigma_1) F^{b}_{\mathrm{I},\lambda_1}}{1 - (\sigma_2/\sigma_1)(\sigma_3/\sigma_4)}, \quad F_{\mathrm{II},\lambda_2} = \frac{F^{a}_{\mathrm{II},\lambda_2} - (\sigma_2/\sigma_1) F^{b}_{\mathrm{II},\lambda_2}}{1 - (\sigma_2/\sigma_1)(\sigma_3/\sigma_4)} \tag{A.3}$$

References

Bogy, D.B., Wang, K.C., 1971. Stress singularities at interface corners in bonded dissimilar isotropic elastic materials. International Journal of Solids and Structures 7, 993–1005.

Chen, D.H., 1992. Analysis for corner singularity in composite materials based on the body force method. Localized Damage II 1, 397–421.

Chen, D.H., Nisitani, H., 1993. Singular stress near the corner of jointed dissimilar materials. ASME Journal of Applied Mechanics 60, 607–613.

Christman, T., Needleman, A., Suresh, S., 1989. An experimental and numerical study of deformation in metal-ceramic composites. Acta Metallurgica 37, 3029–3050.

Dundurs, J., 1967. Effect of elastic constants on stress in a composite under plane deformation. Journal of Composite Materials 1, 310–322.

Needleman, A., 1972. Void growth in an elastic–plastic medium. Journal of Applied Mechanics, 964–970.

Nisitani, H., 1967. The two-dimensional stress problem solved using an electric digital computer. Journal of the Japan Society of Mechanical Engineers 70, 627–632, Bulletin of Japan Society of Mechanical Engineers 11 (1968) 14–23.

Nisitani, H., Noda, N.A., 1984. Stress concentration of a cylindrical bar with a V-shaped circumferential groove under torsion, tension or bending. Engineering Fracture Mechanics 20 (5/6), 743–766.

Nisitani, H., Noguchi, H., Kim, Y.-H., 1993. Fatigue process in short carbon-fiber reinforced polyamid 6.6 under rotating-bending and torsional fatigue. Engineering Fracture Mechanics 45 (4), 497–512.

Noda, N.-A., Kawashima, Y., Moriyama, S., Oda, K., 1996. Interaction of newly defined stress intensity factors for angular corners in a row of diamond-shaped inclusions. International Journal of Fracture 82, 267–295.

Noda, N.-A., Wang, Q., Uemura, Y., Kawashima, Y., 1998. Singular integral equation method in the analysis of interaction between rectangular inclusion. JSME International Journal, Series A 41 (3), 303–308.

Noda, N.-A., Takase, Y., Chen, M., 2000. Generalized stress intensity factors in the interaction between two fibers in matrix. International Journal of Fracture 103, 19–39.

Noda, N.-A., Genkai, T., Wang, Q., 2003. Intensity of singular stress fields at the end of a cylindrical inclusion. ASME Journal of Applied Mechanics 70 (4), 487–495.

Tvergaard, V., 1981. Influence of voids on shear band instabilities under plane strain conditions. International Journal of Fracture 17, 389–407.

Tvergaard, V., 1990. Analysis of tensile properties for a whisker-reinforced metal–matrix composite. Acta Metall 38, 185–194.